Encoder-less Direct Torque Controller for Limited Speed Range Applications of Brushless Doubly-Fed Reluctance Motors

Milutin Jovanović, *Senior Member, IEEE*, Jian Yu, and Emil Levi, *Senior Member, IEEE*

***Abstract*— The paper proposes a direct torque control (DTC) algorithm suitable for low variable frequency operation of the BDFRM and considers aspects of its practical implementation. The simulation and experimental results show that a small BDFRM prototype can successfully operate down to zero supply frequency of the inverter-fed (secondary) winding, unlike cage induction or many other AC machines with DTC. This BDFRM advantage is a consequence of using a flux estimation technique not relying on the secondary voltage integration and therefore avoiding the well-known problems at low secondary frequencies, typical for the BDFRM normal operation. The developed algorithm also offers the prospect for optimising the machine performance in a manner similar to conventional vector controllers but with control actions executed in a stationary reference frame as usual for all traditional DTC methods. The maximum torque per inverter ampere (MTPIA) control strategy has been chosen as a case study.**

***Index Terms*— Direct Torque Control, Brushless Doubly Fed Reluctance Machines.**

I. Introduction

THE Brushless Doubly Fed Reluctance Machine (BDFRM) allows the use of a partially rated inverter which lowers the cost of an electric drive. However, due to the increased cost of the machine itself (to be discussed in the following) and the declining power electronic prices, the capital cost savings are only pronounced in larger power applications with restricted variable speed capability (such as pumps [1], [2] and wind turbines [2], [3]) where the converter size can be further reduced (for a typical speed range of 2:1, the converter real power rating can be limited to about 25% of the machine rating [2], [4], [5], [6]). In these systems the supply quality would also be less affected by the lower harmonic magnitudes generated by the smaller inverter.

The BDFRM has two standard sinusoidally distributed stator windings of different pole numbers and applied frequencies - the grid connected 'primary' or 'power' winding, and the inverter-fed 'secondary' or the 'control' winding (Fig. 1). In order to provide rotor position dependent magnetic coupling between them, a pre-requisite for the machine to produce useful torque, the rotor must have half the total number of stator poles. Therefore, unlike a conventional machine, design

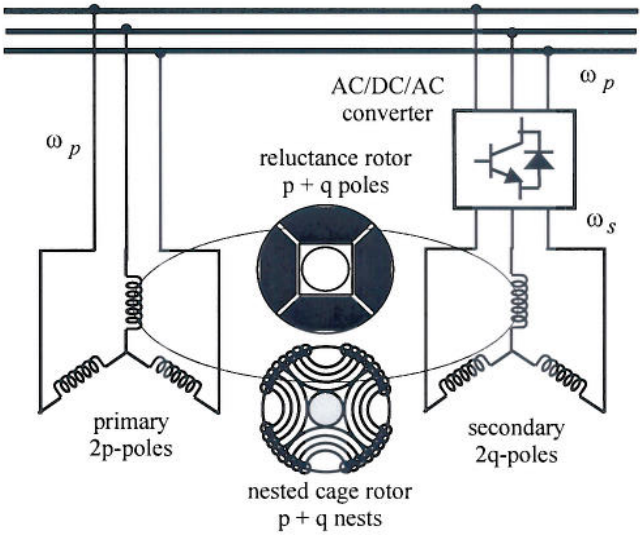

Fig. 1. A conceptual diagram of the BDFRM and the BDFIM

solutions with odd rotor pole numbers (for example, it is 3 in case of a 4/2-pole stator) are possible [3], [7]. Despite this, the 'proof-of-concept' BDFRMs with 6/2-pole stator windings and a 4-pole rotor have been almost exclusively reported in the literature.

In comparison with other members of the slip power recovery family of machines, the BDFRM has several advantages. Owing to its brushless structure, it is more reliable and requires lower maintenance than the traditional doubly-excited wound rotor induction machine (DEWRIM), which can be of the utmost importance for off-shore wind power generation. The brushless doubly-fed induction machine (BDFIM), a BDFRM counterpart, has the same double-winding stator as the BDFRM but because of a special cage rotor (Fig. 1) [8], it should be less efficient[1] [9] and more difficult to model/control[2] than the BDFRM whose rotor (Fig. 1) can be similar to the modern cageless synchronous reluctance machine (SyncRel) [4]. It has been shown in [4] that, as with the SyncRel, the BDFRM performance generally improves with increasing rotor saliency-ratio. This property is important as the deployment of

Dr M.G.Jovanović is with the School of Computing, Engineering and Information Sciences, University of Northumbria at Newcastle, Newcastle upon Tyne NE1 8ST, United Kingdom. (Email: milutin.jovanovic@unn.ac.uk)

Dr J.Yu is with the Scottish-Southern Energy, System Planning, Perth PH1 3AQ, United Kingdom. (Email: james.yu@scottish-southern.co.uk)

Professor E.Levi is with the School of Engineering, John Moores University, Liverpool L3 3AF, United Kingdom. (Email: e.levi@livjm.ac.uk)

[1]The comparative analysis of the two machines built in the same stator frame has demonstrated similar or better overall performance of the BDFRM in doubly-fed and synchronous (i.e. with a DC fed secondary winding) operating modes [9].

[2]In contrast to the BDFIM, field-oriented (vector) control of the primary reactive power and electromagnetic torque is inherently decoupled in the BDFRM (so is with the DEWRIM) [10], [11].

commercially available SyncRel rotors can make the BDFRM manufacture more cost-effective.

The main limitations of the BDFRM can all be attributed to the unusual operating principle and the fact that the flux sidebands (resulting from the modulation process of the stator mmf-s through the rotor), and not the fundamental flux component, participate in the electro-mechanical energy conversion [5], [6], [12]. The magnetic coupling between the BDFRM windings is consequently weaker (i.e. the leakage inductances are higher) relative to the equivalent induction machine or the SyncRel leading to compromised power factor performance [2], [10], an inferior torque per volume and the requirement for a larger BDFRM for the same torque output [4]. The use of the BDFRM therefore offers a trade-off between the size (i.e. VA rating) of the supply converter and the machine. The latest advances in BDFRM rotor design have however indicated the potential of achieving competitive and even superior performance to the induction machine [13] and warrant further BDFRM investigation.

The existing BDFRM control literature has been mostly concerned with the theoretical analysis of various control strategies for optimum machine operation [4], [2], and the development of associated vector controllers either with [3], [11] or without [14] using a shaft position sensor. Scalar control aspects for low performance 'pump-alike' applications of the BDFRM have been also considered [2]. However, while a number of journal papers dealing with position sensor [15], [16], [17], [18], [19] or sensorless [20], [19], [21], [22] field-oriented control of the inverter-fed DEWRIM has appeared in the last ten years, no or very little practical work has been published on direct torque control (DTC) of the BDFRM or other doubly-fed machines (DFMs). A DTC algorithm for the BDFRM proposed by the authors in [23] has only been studied by computer simulations. An alternative DTC technique for the BDFIM was rotor frame based, required the use of a shaft sensor for torque control and it was very complex and time consuming for the DSP implementation [24]. A DTC scheme recently presented in [25] for a classic doubly-fed wind turbine induction generator (DFIG) has also not been experimentally verified. To the best of the authors' knowledge, the only test validation of sensorless DTC for DFMs has been reported in [26] but for the DFIG. While a viable, parameter-independent DTC algorithm for unity power factor control of the DFIG in wind power applications has been developed, the sustained synchronous speed operation of the machine has not been demonstrated.

The primary purpose of this paper is to provide a novel contribution in this area, by proposing a sensorless[3] DTC algorithm (Fig. 2) that can make the BDFRM preferable to other more traditional inverter-fed AC machines foremost in terms of the possibility of stable and reliable operation down to zero applied frequency of the secondary winding. It will be shown in the paper how one can optimise torque per secondary (inverter) ampere (or any other performance parameter of interest) of the machine for a given torque despite the essentially scalar nature of the DTC and the fact that it

[3]A shaft position sensor is only used for speed control.

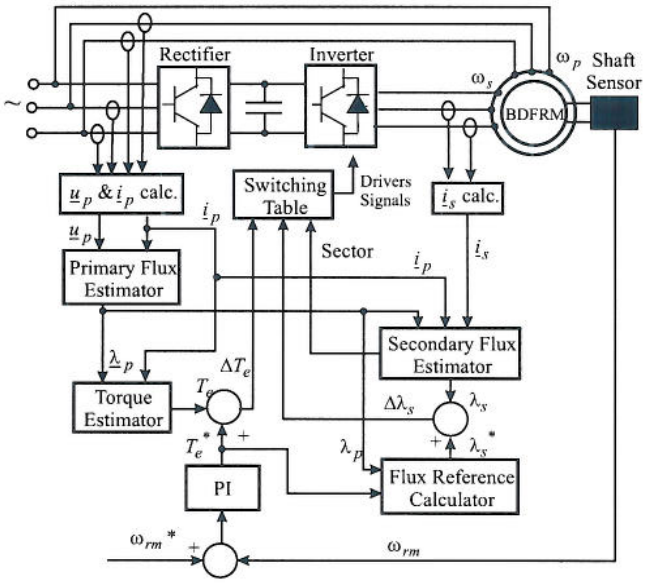

Fig. 2. A simplified diagram of a BDFRM drive with DTC

is executed in a stator frame as usual for all the conventional DTC methods. In this sense, the material to be presented can serve as a good reference for DTC studies on both the BDFRM and DEWRIM due to close modeling similarities between these two conceptually different machines.

II. Dynamic Model

The space-vector equations in a stationary reference frame and the fundamental angular velocity relationship for the machine using standard notation and assuming motoring convention are [27], [12], [5]:

$$\underline{u}_p = R_p\underline{i}_p + \frac{d\underline{\lambda}_p}{dt} = R_p\underline{i}_p + \left.\frac{d\underline{\lambda}_p}{dt}\right|_{\theta_p \text{ const}} + j\omega_p\underline{\lambda}_p \quad (1)$$

$$\underline{u}_s = R_s\underline{i}_s + \frac{d\underline{\lambda}_s}{dt} = R_s\underline{i}_s + \left.\frac{d\underline{\lambda}_s}{dt}\right|_{\theta_s \text{ const}} + j\omega_s\underline{\lambda}_s \quad (2)$$

$$\underline{\lambda}_p = \lambda_p e^{j\theta_p} = L_p\underline{i}_p + L_{ps}\underline{i}_s^* e^{j\theta_r} \quad (3)$$

$$\underline{\lambda}_s = \lambda_s e^{j\theta_s} = L_s\underline{i}_s + L_{ps}\underline{i}_p^* e^{j\theta_r} \quad (4)$$

$$\omega_r = d\theta_r/dt = p_r\omega_{rm} = \omega_p + \omega_s = (1-s)\omega_p \quad (5)$$

where '*' denotes the complex conjugate, $L_{p,s,ps}$ are the 3-phase inductances of the primary and secondary windings [4], [5], ω_{rm} is the rotor mechanical angular velocity, p_r is the rotor pole number, $\omega_{p,s}$ are the applied frequencies to the windings (rad/s) and $s = -\omega_s/\omega_p$ is the 'generic' slip. Notice from (5) that $\omega_s > 0$ for super-synchronous operation (when $s < 0$ by analogy to induction generators) and $\omega_s < 0$ if the machine is operated below the synchronous speed[4] ($s > 0$ here as with induction motors). The negative secondary frequency in sub-synchronous mode indicates the opposite phase sequence of the secondary winding to the primary one.

[4]This speed corresponds to the DC secondary winding (when $\omega_s = s = 0$), which plays the role of the field winding of a classical wound rotor synchronous machine in this case.

III. DTC Strategy

A. Comparisons with Induction Machines

It can be seen that by omitting the differential and '$e^{j\theta_r}$' terms in (1)-(4) one obtains equations similar to the DEWRIM in an arbitrary reference frame rotating at ω_p [5]. The fundamental DTC concepts for the BDFRM can be established from the resulting flux and torque expressions:

$$\underline{\lambda}_p = L_p\underbrace{(i_{pd}+ji_{pq})}_{\underline{i}_p} + L_{ps}\underbrace{(i_{sd}-ji_{sq})}_{\underline{i}_s^*} \tag{6}$$

$$\underline{\lambda}_s = \sigma L_s\underline{i}_s + \underbrace{\frac{L_{ps}}{L_p}\underline{\lambda}_p^*}_{\underline{\lambda}_{ps}} = \sigma L_s(i_{sd}+ji_{sq}) + \underline{\lambda}_{ps} \tag{7}$$

$$T_e = \frac{3p_r}{2\sigma L_s}\left|\underline{\lambda}_{ps}\times\underline{\lambda}_s\right| = \frac{3p_r}{2\sigma L_s}\frac{L_{ps}}{L_p}\lambda_p\lambda_s\sin\delta \tag{8}$$

where $\sigma = 1 - L_{ps}^2/(L_pL_s)$ is the leakage factor (defined as with the induction machine), λ_{ps} is the primary flux linking the secondary winding, and λ_s is the controllable secondary flux magnitude. The angular positions of these phasors (they both rotate at ω_s allowing the machine torque to be developed) are self-evident from Fig.3. Note that λ_p and λ_{ps} are approximately constant due to the primary winding grid connection.

It is important to realise that the mutual flux phasors corresponding to the exponential terms in (3) and (4) rotate at ω_p and ω_s respectively and not ω_s and ω_p as their originating current phasors (Fig.3). This frequency variation is a consequence of the rotor modulating action on the stator mmf waveforms (of different both temporal and spatial pole numbers) and represents the basic torque producing mechanism in the BDFRM [12]. The frequency conversion is carried out through '$e^{j\theta_r}$' as follows from (3)-(5):

$$\underline{i}_s^* e^{j\theta_r} = I_s e^{-j(\omega_s t+\alpha_s)}e^{j(\omega_s+\omega_p)t} = I_s e^{j(\omega_p t-\alpha_s)} \tag{9}$$

$$\underline{i}_p^* e^{j\theta_r} = I_p e^{-j(\omega_p t+\alpha_p)}e^{j(\omega_s+\omega_p)t} = I_p e^{j(\omega_s t-\alpha_p)} \tag{10}$$

where (9) and (10) can be treated as the complex conjugates of the actual stationary frame current vectors referred to their complementary winding side but in a frequency (and not transformer) sense. This now explains why are λ_{ps} and λ_s vectors stationary one with respect to the other as previously mentioned.

An immediately obvious observation from (1)-(8) is that a close modelling link exists between the BDFRM and the DEWRIM despite the principally different operating concept. Therefore, the fundamental DTC theory for cage induction machines [28], [29], [30] can serve as a benchmark in the DTC development for the BDFRM bearing in mind that, in a control sense, λ_{ps} and λ_s are analogous to the rotor and stator flux of the induction machine respectively. Once this analogy has been established, it means that hysteresis control of λ_s and torque (via δ i.e. $\theta_s = \delta + \theta_{ps}$ variations as $\theta_{ps} \approx$ const. in the dynamic sense and particularly at low ω_s values being typical for the BDFRM target applications [2], [10]) can be achieved similarly to the induction machine by applying appropriate voltage vectors to the secondary winding so that the desired influence on the control variables is made [23], [31].

The essential difference between the two machines is the possibility of sustained sub-synchronous operation of the BDFRM (the torque and speed are of the same sign i.e. both positive or negative) with the inverter in regenerative mode unlike the cage induction motor which is then under dynamic breaking conditions. In this speed region $\underline{\lambda}_{ps}$ and $\underline{\lambda}_s$ as well as $\underline{i}_s$ all rotate in the opposite (i.e. clockwise) direction to $\underline{\lambda}_p$ (Fig.3) due to the reversed phase sequence of the secondary to the primary winding as mentioned earlier. One can conclude that, owing to its double feeding, the BDFRM (and the DEWRIM) can achieve wider speed ranges if supplied with the same inverter as the cage induction or any other singly-fed machine.

B. Secondary Flux Optimisation

Using (6)-(8) one can derive an expression for determination of the optimum secondary flux reference (λ_s^*) for a particular performance parameter of the machine and a desired torque (T_e^*). For example, the maximum torque per inverter ampere (MTPIA) strategy allows the minimum inverter loading and higher machine efficiency for a given torque [2], [4], [6]. This control objective would be satisfied if the secondary current was only torque producing. Therefore, by setting $i_{sd} = 0$ in (6)-(8), the corresponding λ_s^* can be shown to be:

$$\lambda_s^* = \sqrt{\lambda_{ps}^2 + \left(\frac{\sigma L_{ps}}{1-\sigma}\frac{2T_e^*}{3p_r\lambda_p}\right)^2} \tag{11}$$

Considering that most of the secondary flux comes from the primary side through mutual coupling (represented by $\lambda_{ps} \approx$ const.), the variable torque term in (11) is only a small portion of the λ_s^* magnitude at any load. This means that the machine is virtually fully fluxed even when unloaded and, in this respect, it can respond quickly to load torque changes[5]. Another important implication of the $\lambda_{ps} \approx$ const. condition is that despite the scalar control nature of the DTC method, the machine performance can still be optimised similarly to vector control but, contrary to the latter, in a stationary reference frame so that rotor position information is not required for the torque control (Fig. 2).

C. Flux Estimation

The fact that the BDFRM is normally operated in a narrow range around the synchronous speed ($\omega_{syn} = \omega_p/p_r$) i.e. at small ω_s values (to reduce the size and cost of the supply inverter), prevents the use of a standard voltage integration approach, based on (2), for the secondary flux estimation in the DTC scheme of Fig. 2. The reason for this are well-known problems associated with the adverse resistance variation effects on the estimation accuracy at low applied voltages. Fortunately, as both the BDFRM windings are externally accessible, it is possible to calculate the secondary flux magnitude (λ_s) and its angular position, θ_s (for locating $\underline{\lambda}_s$ orientation in a stator frame i.e. for sector identification) from measurements

[5]There is a trade-off here since the machine transient response is, on the other hand, compromised by the higher leakage inductances compared to the induction machine.

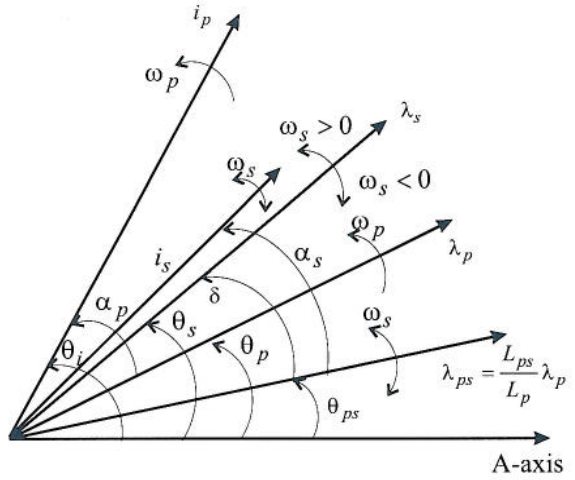

Fig. 3. Characteristic phasors in a stationary reference frame

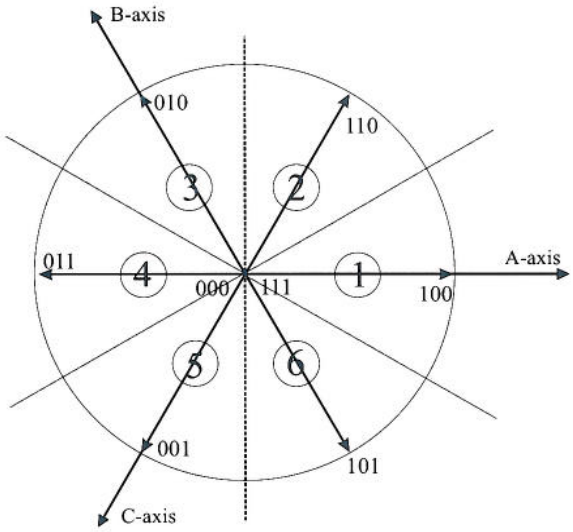

Fig. 4. Secondary voltage vectors and associated $\pi/3$ sectors

of the primary voltages and winding currents using (1), (3) and (4). The relevant expressions for a Y-connected machine with an isolated neutral point (so that $i_c = -i_a - i_b$) and the 'ABC' phase sequence of the windings (Fig. 4), are:

$$\underline{\lambda}_s = \lambda_s e^{j\theta_s} = L_s \underline{i}_s + \frac{\underline{\lambda}_p - L_p \underline{i}_p}{\underline{i}_s^*} \cdot \underline{i}_p^* \tag{12}$$

$$\underline{\lambda}_p = \lambda_p e^{j\theta_p} = \int \left(\underline{u}_p - R_p \underline{i}_p\right) dt \tag{13}$$

where the stationary frame phasors are related to the respective phase quantities as:

$$\underline{X} = X_a + j\frac{X_a + 2X_b}{\sqrt{3}}, \qquad X = u_p, i_p, i_s \tag{14}$$

Note that the price to pay for avoiding the secondary voltage integration in (12) is the increased parameter dependence as the inductances need to be known (see the Appendix). Also, with smaller machines (such as the one considered in this paper) having inherently higher resistances, one has to take into account the primary resistance voltage drop in (13). While $R_p i_p << \lambda_p$ in most situations, for the MTPIA control strategy in particular where i_s is a minimum, even minor inaccuracies in $\underline{\lambda}_p$ estimates, when multiplied by a factor of i_p/i_s in (12), can cause high estimation errors in $\underline{\lambda}_s$. The increased numerical sensitivity of this alternative estimation technique to practical effects (e.g. measurement noise, quantization errors and DC offset introduced by the current and voltage transducers) and parameter knowledge uncertainties has made the MTPIA difficult to realize in real-time as will be shown later.

Finally, it is worth mentioning that sensorless speed control is also feasible as the rotor 'electrical' angle ($\theta_r = p_r \theta_{rm}$) can be deduced from measurements using (3) and (4). Issues related to this have already been addressed by the authors in [31] and won't be repeated in this paper.

D. Torque Estimation

Amongst several equivalent torque expressions for the BDFRM, the best estimates are obtained applying the following one:

$$T_e = \frac{3}{2} p_r \left|\underline{\lambda}_p \times \underline{i}_p\right| = \frac{3}{2} p_r \lambda_p i_p \sin(\theta_i - \theta_p) \tag{15}$$

where λ_p and θ_p are given by (13), and i_p and θ_i immediately follow from (14). The above torque relationship is only dependent[6] on R_p (indirectly through λ_p) and is exclusively a function of the primary quantities having smooth, almost 'ripple-free', waveforms at fixed line frequency. It should be noted that the switching ripples, naturally present in the secondary waveforms, are virtually non-existent on the primary side because of the relatively weak magnetic coupling between the BDFRM windings.

E. Inverter Switching Principles

The outputs of the flux and torque 2-level comparators in the DTC algorithm for the BDFRM (Fig.2) are:

$$\Delta\lambda_s = \begin{cases} 1, & \lambda_s^* - \lambda_s \geq \Delta\lambda \\ 0, & \lambda_s^* - \lambda_s \leq -\Delta\lambda \end{cases} \tag{16}$$

$$\Delta T_e = \begin{cases} 1, & T_e^* - T_e \geq \Delta T \\ 0, & T_e^* - T_e \leq -\Delta T \end{cases} \tag{17}$$

where $\Delta\lambda$ and ΔT indicate the corresponding hysteresis bands, and the meanings of '1' and '0' are respectively the increase and decrease of the secondary flux magnitude and/or instantaneous torque in its actual (not absolute) sense where the torque is assumed positive if acting anti-clockwise. Therefore, if a particular control variable (flux or torque) is out of the bottom band, then '1' should ensure its increase until exceeding the top boundary. At that point, according to (16) and (17), this state is changed to '0' to force the variable value to decrease and stay within the bands for as long as the bottom limit is being hit again when the entire process repeats. The binary codes (with '1' signifying the top device of a leg ON and the bottom one OFF, and vice-versa for '0' bit) and angular positions of the voltage vectors to be applied to the

[6]For control strategies other than the MTPIA, where the primary resistance effects are negligible, this dependence is extremely weak and can be ignored.

TABLE I
OPTIMUM SWITCHING LOOK-UP TABLE

Comparator		Sector					
$\Delta\lambda_s$	ΔT_e	1	2	3	4	5	6
1	1	110	010	011	001	101	100
1	0	101	100	110	010	011	001
0	1	010	011	001	101	100	110
0	0	001	101	100	110	010	011

secondary winding to achieve a specific control action with the minimum number of switchings, are given in Table I and Fig. 4.

Notice from Table I that only the active switching states of the inverter legs (based on the non-zero inverter vectors) have been used for the control. The implementation of this strategy is imperative in the low frequency range as the rate of change of secondary current (and hence torque) would be otherwise severely compromised in zero applied voltage intervals not only by the small back-emf driving the current but also the higher leakage inductances and proportionally larger time constants of the BDFRM. In this sense, there is generally a switching rate trade-off in the BDFRM relative to the DEWRIM. Apart from allowing the fastest transient response from the machine, the 'active vectors' approach has been adopted because of many other advantages it offers including [23], [31]: (a) the DTC scheme becomes simpler and sensorless in nature (the influence of zero vectors, '111' or '000', on the machine torque is different for super- and sub-synchronous operation, and in their presence the torque control would be speed dependent); (b) in keeping with the above observations, the machine synchronous performance (at zero secondary supply frequency) is particularly improved; (c) the real-time implementation is significantly facilitated as the dSPACE® compilers only accept 2-level comparator functional subroutines that are readily available in the Simulink® library (with the zero-vectors included, the torque comparator would have a 3-level structure).

The downside of the technique when compared to using complementary zero vectors is the increased switching frequency and inverter losses for the same torque ripple. Note that due to the ambiguous effect of zero voltages on torque behavior the latter is controlled either in the top (at sub-synchronous speeds) or bottom (at super-synchronous speeds) band as opposed to the situation with the active vectors only when the torque is kept within the both bands irrespective of the speed mode [23]. This means that the torque ripples would be identical in both cases providing that the upper and lower boundaries of the hysteresis torque controller are set to $T_e^* \pm 2\Delta T$ when the zero vectors are applied.

IV. SIMULATIONS

The following plots have been generated by implementing the algorithm in Fig.2 in Simulink® for the MTPIA strategy using the parameters of a BDFRM prototype (see the Appendix). The main reason for choosing this traditional software package is the easy portability of simulation programmes across dSPACE® DSP development platforms. Note also that the circuitry required for starting is not shown in Fig.2. In practice, if a partially-rated inverter is used, auxiliary contactors are usually needed to short the secondary terminals directly or through variable external resistors and start the BDFRM as a wound rotor induction machine avoiding the inverter overloading in this way. Once the machine speed is near synchronous the contactors are opened and the inverter is connected with the control enabled (this occurs at 1.5-s time instant in the simulated plots[7]). An alternative method would be to use the controllable inverter for starting the machine with the shorted primary windings and then self-synchronizing it to the grid for doubly-fed operation, by applying a procedure for commercial DEWRIM drives [20].

Fig.5 shows that the 'theoretical' machine can be effectively controlled in either super-synchronous, synchronous or sub-synchronous mode at different loads owing to the accurate torque and flux control within the specified hysteresis bands (ΔT = 0.25 Nm and $\Delta\lambda$ = 0.005 Wb) as illustrated in Figs. 6-7. The speed transients while loading and unloading the machine, that are clearly visible in Fig.5, are an expected outcome of limited load disturbance rejection abilities of the PI speed controller whose gains have been tuned to achieve desired speed set-points and not to optimally respond to load step changes under steady-state conditions. It should be noted that despite this deficiency of PI regulators the speed excursions are still within acceptable 10% of a particular reference value. Speed control performance can be improved by adaptive PI tuning or, even better, by fuzzy logic techniques offering faster response to sudden load variations than traditional PI approach [32]. The development of either of these strategies is however out of scope of this paper.

V. EXPERIMENTAL RESULTS

The test results presented in this section have been obtained by executing the real-time code (the source Simulink® programme adapted for DSP implementation) at 20 kHz, which also represents the limiting switching frequency from an inverter point of view. Such a high sampling rate (each 50 μs) is due to the computationally effective DTC scheme and fast processing hardware of a powerful dSPACE® system used for its practical realization (refer to the Appendix for details). The speed estimates, derived from the rotor position measurements using a simple Euler's approximation, and the speed controller output (i.e. the torque reference values) are updated at 1 kHz in order to minimize quantization errors and make the control calculations as accurate and fast as possible. The machine response to speed changes will necessarily be sacrificed to some extent by doing this, but the achievable sampling rates will in turn be optimized for high performance DTC. The speed control dynamics can be improved by using a conventional angular velocity observer providing speed estimates at the torque control rate [33]. However, the requirement for knowledge of the drive system inertia would increase parameter dependence and complicate the structure of the DTC algorithm [31].

[7]The BDFRM starting characteristics [23] are very similar to the induction machine and have been omitted for better scaling, and to concentrate one's attention to the control aspects.

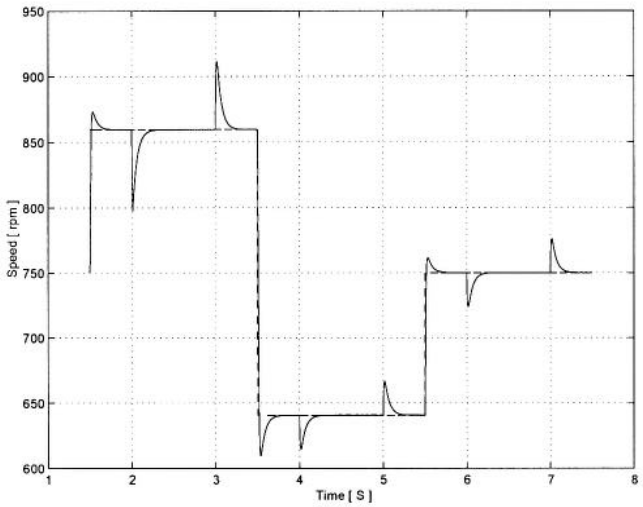

Fig. 5. Simulated machine response to speed/load torque changes

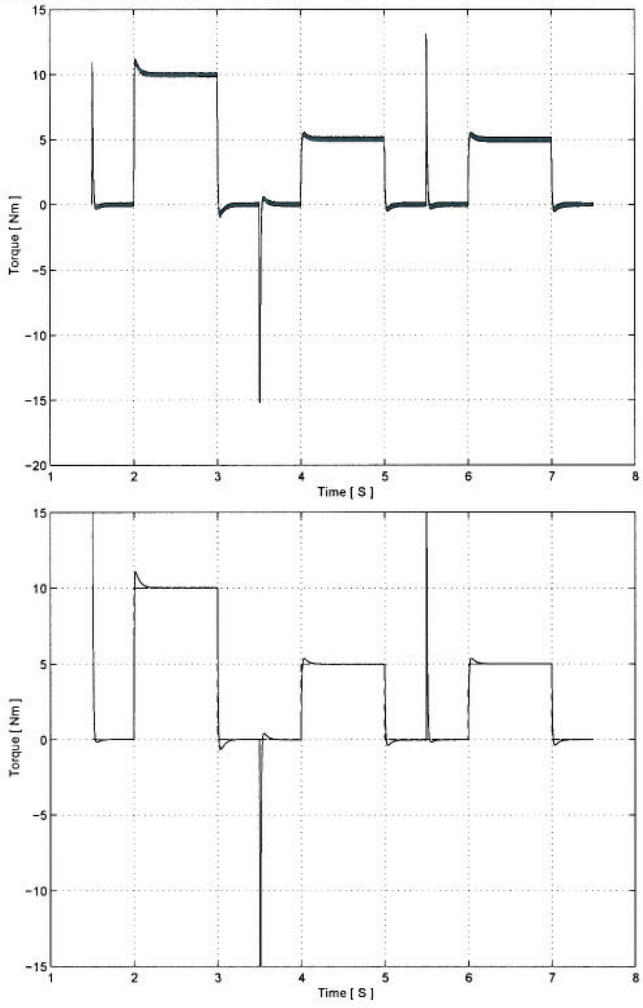

Fig. 6. Simulated torque characteristics: (a) machine torque (top plot); (b) reference torque (bottom plot-solid line) and load torque (bottom plot-dashed line)

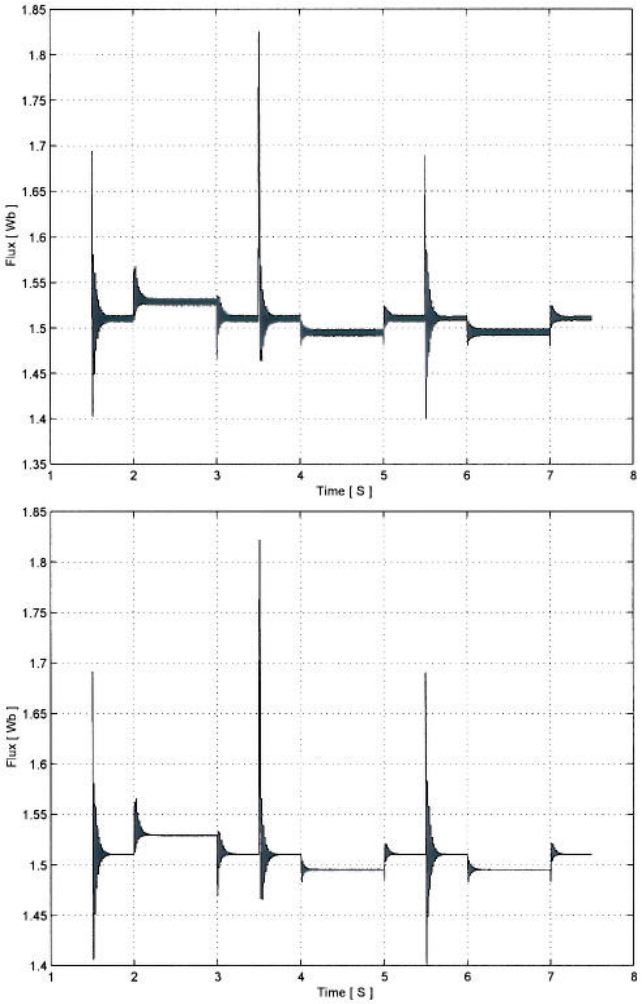

Fig. 7. Simulated Secondary Flux: Actual (top) and MTPIA Reference (bottom)

The main components of a BDFRM test facility have been described in the Appendix. The BDFRM is started as a wound rotor induction machine with the secondary terminals shorted through the inverter i.e. by applying zero voltages ('111' or '000'). This starting method is possible as the inverter supplying the machine is overrated for testing purposes. Otherwise, i.e. in case of a partially rated converter, one would need to follow the starting procedure outlined in the previous section. Once the machine has reached its steady sub-synchronous speed determined by the no-load slip value, the control is enabled (at 5-s time instant in the plots presented). The DTC performance has been intentionally examined in a narrow speed range from 72.08 rad/s (688 rpm) to 85 rad/s (812 rpm) i.e. 6.46 rad/s (62 rpm) below and above the synchronous speed, for two main reasons: (a) because this analysis is of most interest to the BDFRM target applications; and (b) to illustrate the advantages of the proposed DTC method in the low frequency region being the most difficult to handle with traditional DTC. The flux and torque hysteresis bands have been set to $\Delta\lambda = 0.05$ Wb and $\Delta T = 0.5$ Nm respectively resulting in the total bandwidths of 0.1 Wb and

1 Nm according to (16) and (17).

The simulation results, shown in the remainder of this section, have been generated under similar conditions as the experimental. Whenever possible, the respective plots are presented in the same figures for easier comparison. It should be emphasized that given the absence of practical effects of iron and mechanical losses in the simulations, the simulated load torque is set to the corresponding experimental torque reference (5 Nm) in order to best emulate the real-time situation.

Fig. 8 demonstrates the BDFRM ability to operate successfully down to synchronous speed (78.54 rad/s = 750 rpm) when the secondary frequency is zero (from about 17-s onward). It is well-known that the low frequency operation is troublesome for many inverter-fed DTC machines, the cage induction motors being a typical example. It can be seen that the simulated and real machine response to the requested speed changes is almost identical, the latter being somewhat slower during the speed reversal for the reasons explained below.

The good speed controller performance is a consequence of the accurate tracking of a desired torque trajectory, especially in steady-state as illustrated in Figs. 9 and 10. The same figures also show a good overall agreement between the simulation and experimental torque waveforms. The shortage of braking torque in Fig. 10 while varying the machine speed from above to below synchronous is due to the erroneous secondary flux estimates manifesting themselves in the instantaneous flux being controlled way out the specified hysteresis band which is more than evident from Fig. 12. It is important to add though that despite the clearly higher ripples, the average flux seems to be kept at the correct reference values. These estimation difficulties arise from the sensitivity effects of the flux observer under the MTPIA conditions discussed in Section III-C. Unlike the experiments, the simulated secondary flux is maintained strictly within the bands as follows from Fig. 11.

The impact of poor flux control on the machine torque dynamics is not that significant and torque variations, while still out of the band, are much smaller in relative sense as illustrated in Fig.10. This increased 'immunity' of the torque controller can most likely be attributed to using (15) for torque calculations (see Section III-D). Notice also from Fig.10 that the estimated electromagnetic torque is well above zero in steady-state for the unloaded machine since no-load losses have not been accounted for in the control model. This well-known phenomenon of uncompensated control reflects on the speed controller asking for more torque to be produced by the machine to cover the losses. The same is the reason for the varying flux reference in Fig. 12 as opposed to the simulation conditions where the torque (Fig. 9) and flux (Fig. 11) references are both speed independent i.e. constant. The measurements of the primary winding real power input in the open-circuit test with the machine rotating at no-load speed have confirmed this conjecture. It turned out that this power indeed corresponded well to the speed and torque values in Figs.8 and 10.

The respective secondary current waveforms for the three characteristic operating modes of the machine are shown in Figs.13 and 14. As indicated above, the considered reference speeds are 6.46 rad/s (62 rpm) above and below the synchronous meaning that the secondary supply frequency is $f_s = 4 \cdot 6.46/2\pi = 4.11$ Hz and the current cycle 0.24 s in both cases according to (5). A close inspection of the plots in Fig.13 confirms this remark. Another observation from the same figure, related to the machine fundamental operating principles, is the opposite phase sequence of the currents in the two modes: at super-synchronous speed it is positive (as in the primary winding) i.e. Red-Yellow-Blue, and at sub-synchronous speed it is negative i.e. Red-Blue-Yellow since $\omega_s < 0$ in this speed region (refer to Section II). Note also that the current magnitudes are slightly higher in super- than in sub-synchronous mode since more torque is required from the machine in the first case as follows from Fig.10. Finally, Fig.14 represents the synchronous speed operation with DC secondary currents adding up to zero in average sense (though this is difficult to see from the noisy waveforms) as expected for a winding with an isolated neutral point.

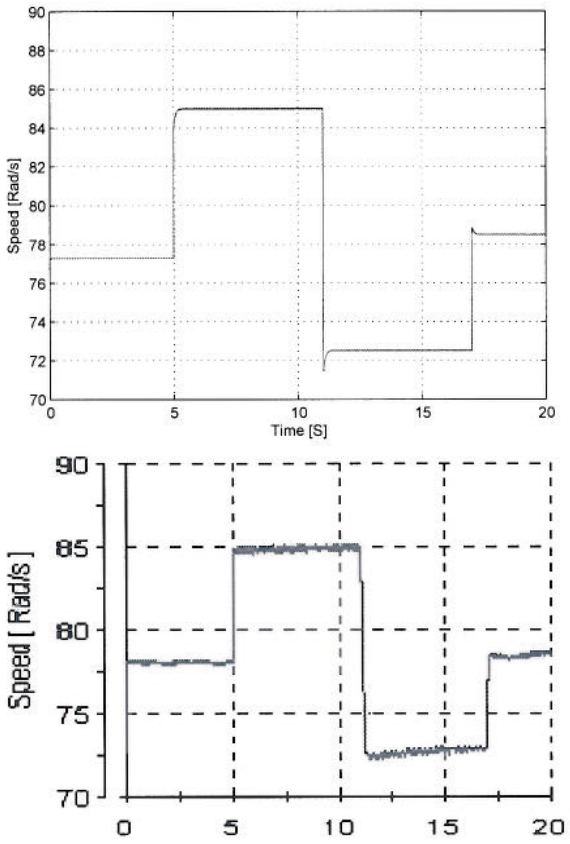

Fig. 8. Speed waveforms: simulated (top) and experimental (bottom)

VI. Conclusions

A new DTC scheme for the BDFRM, that is also applicable to the DEWRIM, has been developed and its effectiveness at different speeds down to zero secondary winding frequency verified by computer simulations and experimentally on a small BDFRM prototype. Such properties of the algorithm have been achieved by estimating the secondary flux indirectly through primary quantities without using the inverter output or

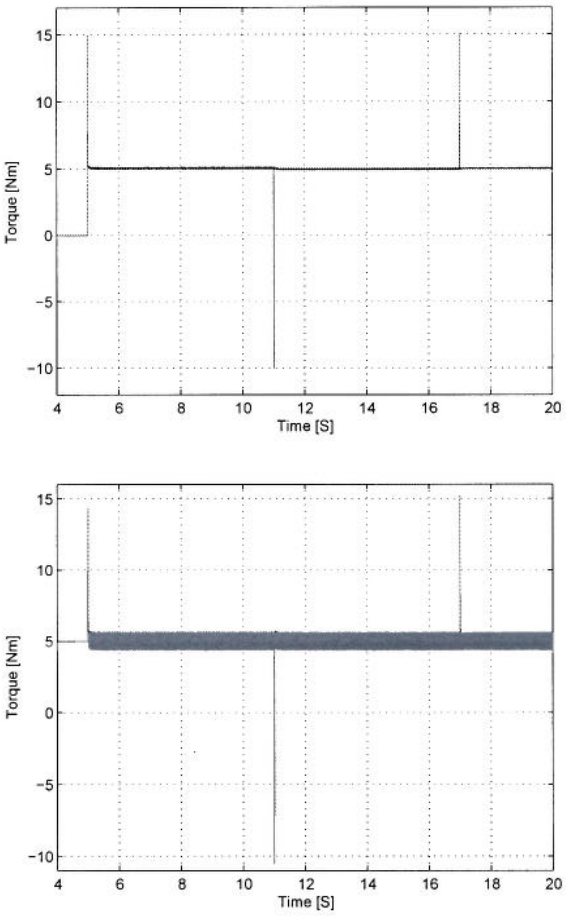

Fig. 9. Simulated torque: reference (top) and actual (bottom)

DC link voltage measurements. The presented test results have however demonstrated that while the low frequency secondary voltage integration problems of conventional DTC schemes have been avoided, the secondary flux estimation errors have not been eliminated (at least not for the MTPIA control strategy considered) due to the pronounced sensitivity issues associated with the proposed flux estimation technique. It is interesting that the torque controller has been shown to be robust to these flux control inaccuracies allowing satisfactory overall performance of the machine. This suggests the possibility of designing a simpler DTC based speed control system without a secondary flux control loop.

The paper has opened up opportunities for further research in the DTC area not only on the BDFRM but also on the DEWRIM. Apart from investigating the means for overcoming the limitations of the existing DTC algorithm, potential directions for future work could include the implementation of other control strategies for the machine(s) and/or the development of improved control schemes with core loss compensation for adjustable speed drives with limited speed ranges and/or variable speed constant frequency wind power applications where the BDFRM might potentially find its wider use as an attractive cost-effective brushless candidate.

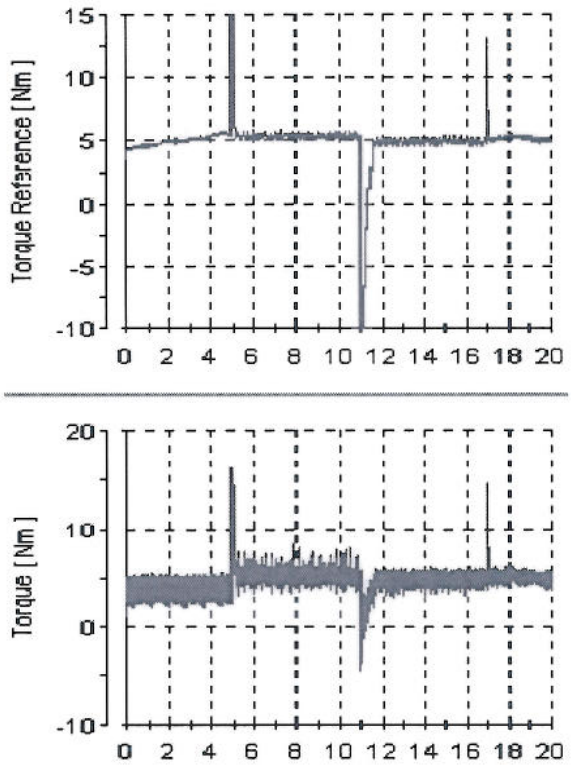

Fig. 10. Torque test results: desired (top) and estimated (bottom)

APPENDIX
BDFRM TEST RIG

The laboratory test system for a 'proof-of-concept' BDFRM driving an 'off-the-shelf' DC load machine is presented in Fig.15. The 6-pole primary and 2-pole secondary windings are both rated at 1.5 kW, 2.5 A, 415 V, 50 Hz. The 4-pole axially-laminated reluctance rotor [23] and the stator have been custom designed and built. The machine construction is far from optimal as the main focus of the project being undertaken has been on control and not design aspects. A standard IGBT voltage source inverter supplying the secondary winding is controlled by a high performance DS1103 PPC controller board from dSPACE®. An incremental encoder with 5000 ppr (increased to 20000 ppr by the 4-fold pulse counting), mounted on the DC side of the drive, has been used for shaft position sensing and speed detection.

The BDFRM parameters of importance for the control have been identified by applying off-line testing methods for conventional slip ring induction machines [9]. The actual resistances (measured by a simple DC test) and 3-phase inductances of the windings are: $R_p = 10.7\Omega$, $R_s = 12.68\Omega$, $L_p = 0.407$H, $L_s = 1.256$H and $L_{ps} = 0.57$H. The values are somewhat higher than usual mainly due to the small gage copper wire employed and consequent larger number of turns of the windings (especially the secondary).

REFERENCES

[1] B.Gorti, D.Zhou, R.Spée, G.Alexander, and A.Wallace, "Development of a brushless doubly-fed machine for a limited speed pump drive in a waste water treatment plant," *Proc. of the IEEE-IAS Annual Meeting*, pp. 523–529, Denver,Colorado,October 1994.

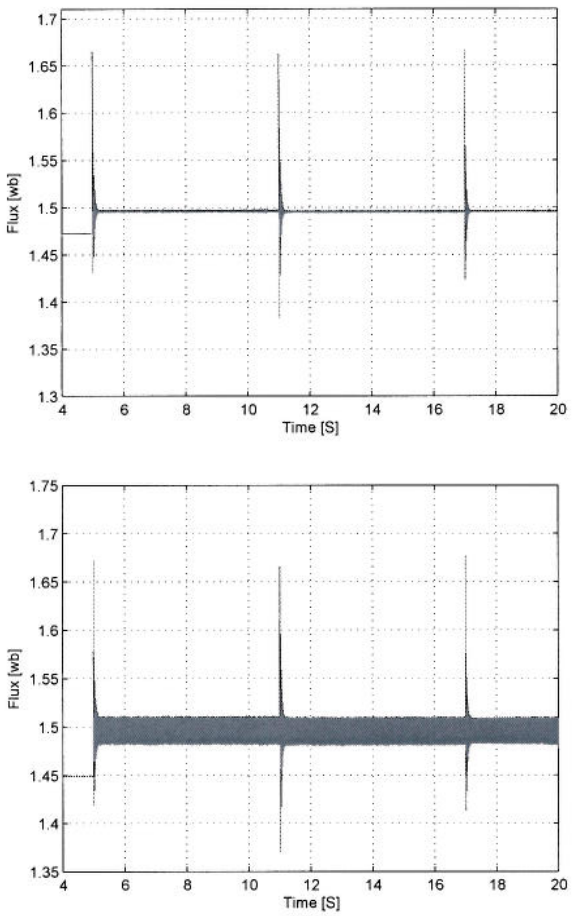

Fig. 11. Secondary flux from simulations: desired (top) and observed (bottom)

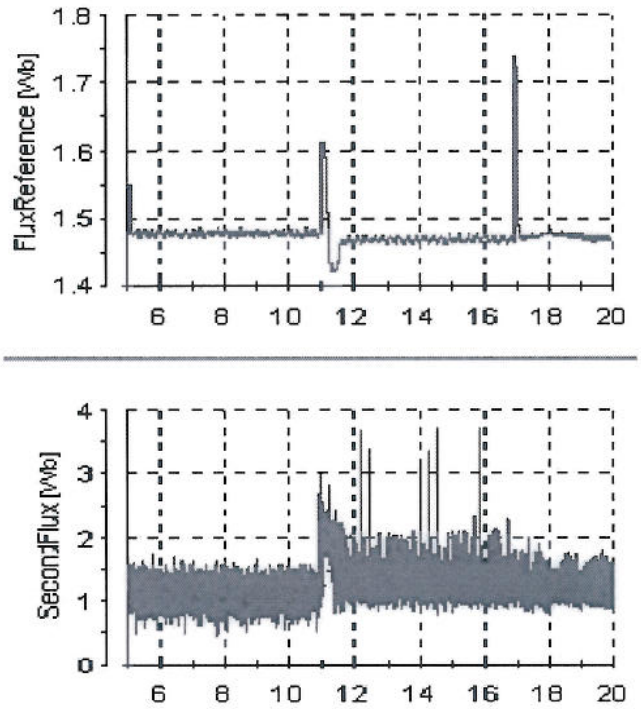

Fig. 12. Test results for Secondary Flux: desired (top) and observed (bottom)

[2] M.G.Jovanović, R.E.Betz, and J.Yu, "The use of doubly fed reluctance machines for large pumps and wind turbines," *IEEE Transactions on Industry Applications*, vol. 38, no. 6, pp. 1508–1516, Nov/Dec 2002.

[3] L. Xu and Y. Tang, "A novel wind-power generating system using field orientation controlled doubly-excited brushless reluctance machine," *Proc. of the IEEE IAS Annual Meeting*, Houston, Texas, October 1992.

[4] R.E.Betz and M.G.Jovanović, "The brushless doubly fed reluctance machine and the synchronous reluctance machine - a comparison," *IEEE Transactions on Industry Applications*, vol. 36, no. 4, pp. 1103–1110, July/August 2000.

[5] ——, "Introduction to the space vector modelling of the brushless doubly-fed reluctance machine," *Electric Power Components and Systems*, vol. 31, no. 8, pp. 729–755, August 2003.

[6] ——, "Theoretical analysis of control properties for the brushless doubly fed reluctance machine," *IEEE Transactions on Energy Conversion*, vol. 17, no. 3, pp. 332–339, Sept 2002.

[7] L. Xu, "Analysis of a doubly-excited brushless reluctance machine by finite element method," *Proceedings of the IEEE IAS Annual Meeting*, pp. 171–177, 1992.

[8] S. Williamson, A. Ferreira, and A. Wallace, "Generalised theory of the brushless doubly-fed machine. part 1: Analysis," *IEE Proc.-Electric Power Applications*, vol. 144, no. 2, pp. 111–122, March 1997.

[9] F.Wang, F.Zhang, and L.Xu, "Parameter and performance comparison of doubly-fed brushless machine with cage and reluctance rotors," *IEEE Transactions on Industry Applications*, vol. 38, no. 5, pp. 1237–1243, Sept/Oct 2002.

[10] M.G.Jovanović and R.E.Betz, "Power factor control using brushless doubly fed reluctance machines," *Proc. of the IEEE-IAS Annual Meeting*, Rome, Italy, October 2000.

[11] L. Xu, L. Zhen, and E. Kim, "Field-orientation control of a doubly excited brushless reluctance machine," *IEEE Transactions on Industry Applications*, vol. 34, no. 1, pp. 148–155, Jan/Feb 1998.

[12] Y. Liao, L. Xu, and L. Zhen, "Design of a doubly-fed reluctance motor for adjustable speed drives," *IEEE Transactions on Industry Applications*, vol. 32, pp. 1195–1203, Sept/Oct 1996.

[13] E.M.Schulz and R.E.Betz, "Optimal torque per amp for brushless doubly fed reluctance machines," *CD-ROM Proc. of IEEE-IAS Annual Meeting*, Hong Kong, October 2005.

[14] Y. Liao and C. Sun, "A novel position sensorless control scheme for doubly fed reluctance motor drives," *IEEE Transactions on Industry Applications*, vol. 30, no. 5, pp. 1210–1218, Sept/Oct 1994.

[15] Y. Tang and L. Xu, "Vector control and fuzzy logic control of doubly fed variable speed drives with DSP implementation," *IEEE Trans. on Energy Conversion*, vol. 10, no. 4, pp. 661–668, December 1995.

[16] Y.Tang and L.Xu, "A flexible active and reactive power control strategy for a variable speed constant frequency generating system," *IEEE Transactions on power electronics*, vol. 10, no. 4, pp. 472–478, July 1995.

[17] L.Xu and W.Cheng, "Torque and reactive power control of a doubly fed induction machine by position sensorless scheme," *IEEE Transactions on Industry Applications*, vol. 31, no. 3, pp. 636–642, May/June 1995.

[18] R.Pena, J.C.Clare, and G.M.Asher, "Doubly fed induction generator using back-to-back PWM converters and its application to variable-speed wind-energy generation," *IEE Proc. - Electr. Power Appl.*, vol. 143, no. 3, pp. 231–241, May 1996.

[19] B.Hopfensperger, D.J.Atkinson, and R.A.Lakin, "Stator-flux-oriented control of a doubly-fed induction machine with and without position encoder," *IEE Proc. - Electr. Power Appl.*, vol. 147, no. 4, pp. 241–250, July 2000.

[20] L.Morel, H.Godfroid, A.Mirzaian, and J.M.Kauffmann, "Double-fed induction machine: Converter optimisation and field oriented control without position sensor," *IEE Proc. - Electr. Power Appl.*, vol. 145, no. 4, pp. 360–368, July 1998.

[21] R. Datta and V.T.Ranganathan, "A simple position-sensorless algorithm for rotor-side field-oriented control of wound-rotor induction machine," *IEEE Transactions on Industrial Electronics*, vol. 48, no. 4, pp. 786–793, August 2001.

[22] R.Cardenas, R.Pena, G.Asher, J.Clare, and J.Cartes, "MRAS observer for doubly fed induction machines," *IEEE Transactions on Energy Conversion*, vol. 19, no. 2, pp. 467–468, June 2004.

[23] M.G.Jovanović, J.Yu, and E.Levi, "Direct torque control of brushless

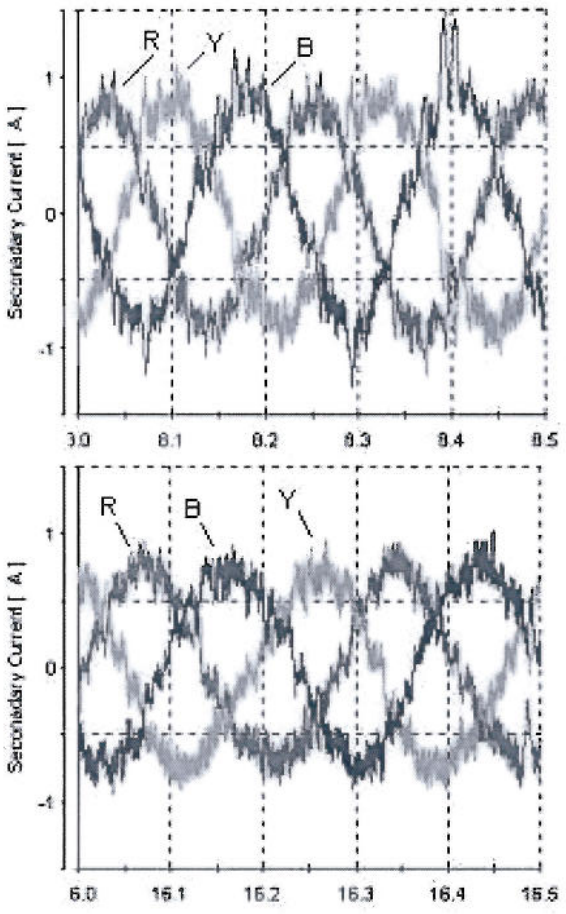

Fig. 13. Measured secondary currents in super-synchronous (top) and sub-synchronous mode (bottom)

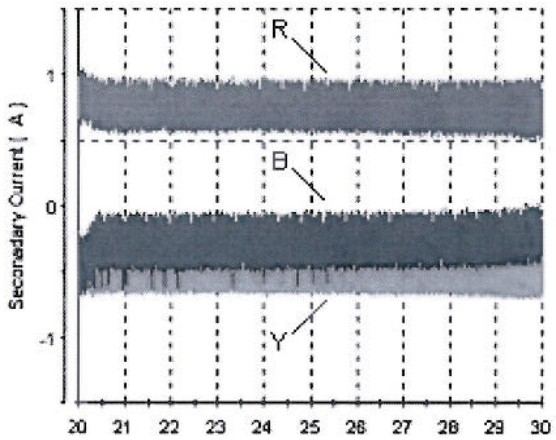

Fig. 14. Measured secondary currents at synchronous speed

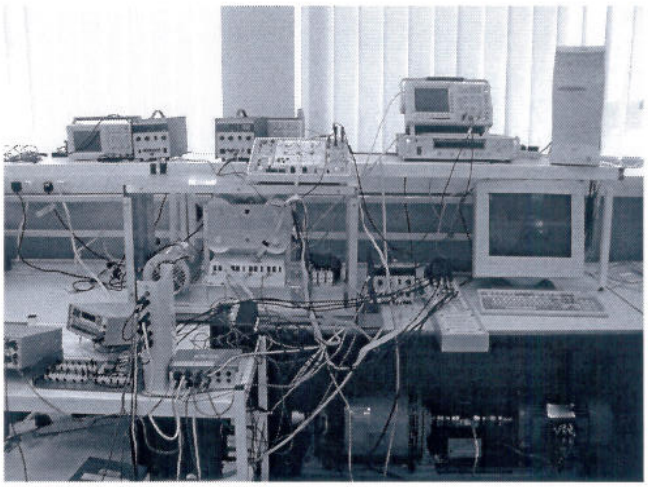

Fig. 15. BDFRM Test System

doubly fed reluctance machines," *Electric Power Components and Systems*, vol. 32, no. 10, pp. 941–958, October 2004.

[24] W.R.Brassfield, R.Spee, and T.G.Habetler, "Direct torque control for brushless doubly-fed machines," *IEEE Transactions on Industry Applications*, vol. 32, no. 5, pp. 1098–1104, 1996.

[25] S.Arnalte, J.C.Burgos, and J.L.Rodriguez-Amenedo, "Direct torque control of a doubly-fed induction generator for variable speed wind turbines," *Electric power components and systems*, vol. 30, pp. 199–216, 2002.

[26] R. Datta and V.T.Ranganathan, "Direct power control of grid-connected wound rotor induction machine without rotor position sensors," *IEEE Transactions on Power Electronics*, vol. 16, no. 3, pp. 390–399, May 2001.

[27] F. Liang, L. Xu, and T. Lipo, "D-q analysis of a variable speed doubly AC excited reluctance motor," *Electric Machines and Power Systems*, vol. 19, no. 2, pp. 125–138, March 1991.

[28] I.Takahashi and T.Noguchi, "A new quick-response and high-efficiency control strategy of an induction machine," *IEEE Transactions on Industry Applications*, vol. IA-22, no. 5, pp. 820–827, Sept/Oct 1986.

[29] I.Takahashi and Y.Ohmori, "High performance direct torque control of an induction motor," *IEEE Transactions on Industry Applications*, vol. 25, no. 2, pp. 257–264, Mar/Apr 1989.

[30] P. Vas, *Sensorless Vector and Direct Torque Control*. Oxford University Press, 1998, ISBN 0-19-856465-1.

[31] M.G.Jovanović, J.Yu, and E.Levi, "A doubly-fed reluctance motor drive with sensorless direct torque control," *IEEE International Electric Machines and Drives Conference (IEMDC)*, Madison, Wisconsin, June 2003.

[32] Z. Ibrahim and E. Levi, "A comparative analysis of fuzzy logic and PI speed control in high-performance AC drives using experimental approach," *IEEE Transactions on Industry Applications*, vol. 38, no. 5, pp. 1210–1218, Sept/Oct 2002.

[33] R. Lorenz and K. Patten, "High-resolution velocity estimation for all-digital, ac servo drives," *IEEE Trans. on Industry Applications*, vol. IA-27, no. 4, pp. 701–705, July/August 1991.

Milutin Jovanović received the Dipl.Eng and M.E.E. degrees from the University of Belgrade, Yugoslavia, in 1987 and 1991 respectively, and the Ph.D. degree from the University of Newcastle, Australia, in 1997. He is currently a Senior Lecturer in the School of Computing, Engineering and Information Sciences, University of Northumbria at Newcastle, UK. His main interests are in the areas of electrical machines and drives, and renewable energy systems. Dr. Jovanović has published more than 70 papers in eminent journals and conference proceedings.

Jian Yu received his B.E. and M.Sc. degrees from the Harbin Institute of Technology, China and Newcastle University, UK in 1998 and 2000 respectively, and the Ph.D. degree from the University of Northumbria at Newcastle, UK, in 2004. He was with PB Power in 2004, and currently is a system planning engineer of the Scottish-Southern Energy. His main research interests are doubly-fed machines, energy transmission and wind power generation.

Emil Levi received the Diploma degree from the University of Novi Sad, Yugoslavia, and the MSc and the PhD degree from the University of Belgrade, Yugoslavia in 1982, 1986 and 1990, respectively. He joined Liverpool John Moores University, UK in 1992 as a Senior Lecturer, where, since 2000 he has been a Professor of Electric Machines and Drives. His main areas of research interest are modeling and simulation of electric machines, control of high performance drives and power electronic converters. He has published over 200 journal and conference papers.